Appl Phys B (2009) 94: 345–353
DOI 10.1007/s00340-008-3273-2

**Applied Physics B**
**Lasers and Optics**

# Molecular relaxations in mixtures of $O_2$ with $CO_2$ observed on laser-induced gratings

**W. Hubschmid**

Received: 23 July 2008 / Revised version: 26 August 2008 / Published online: 15 November 2008


**Abstract** Laser-induced gratings in mixtures of $O_2$ with $CO_2$ were formed by excitation of the $O_2$ molecules to the singlet state $b^1\Sigma_g^+(v'=0)$. Density changes from heat release and from electrostriction, and variation of electric polarizability by excitation of molecules contribute to the grating. For modeling the relaxation of the excited $O_2$ molecules, a three-step process is assumed: Fast heat release with respect to the rotational states first, then medium fast electronic de-activation with excitation of vibrational states of the $O_2$ and $CO_2$ molecules, and then the final slow heat release processes. The observed temporal evolution of the diffraction efficiency of the grating agrees rather well with modeling. Average rates of the final relaxations and the value of the polarizability of the singlet state $b^1\Sigma_g^+(v'=0)$ are determined in this way.

**PACS** 42.65.Es · 43.35.Sx · 34.50.Gb

## 1 Introduction

If two beams of a pulsed laser or of another coherent light source (below just called "light source") overlap in some volume of a medium (gas or other), by various processes a transient laser-induced grating (LIG), i.e., an object with spatially periodic refractive index, is formed; see, e.g., [2, 15]. In the cases investigated here, the beams are irradiated on the overlap volume with a small angle (about 1°). In this way, the interspaces between the grating fringes become rather large, much larger than the wavelengths of the light source. Thus, various dissipation processes (viscosity, thermal conductivity, and mass diffusion) degrade the grating at a relatively small rate. On the other hand, gratings formed by beams with small crossing angles have enlarged overlap volumes for focussed and unfocussed beams. Thus, the spatial resolution of measurements is reduced. This, however, is only a disadvantage for measurement of local quantities but not for measurements of matter and process data, as is mainly aimed at by the investigations described in this article.

The temporal evolution of the diffraction efficiency of the LIG is observed by a probe beam (usually of a cw-laser) and measured by some detector, usually a photomultiplier. This technique of time-resolved LIG can be used to investigate the temporal evolution of the heat release from relaxation processes, which occur after light absorption causing excitation of molecules in the medium. Relaxation rates and polarizabilities of excited states can be determined in this way. Mass diffusion within the grating sets an upper limit for the time scale where the technique of time-resolved LIG can still be applied. It is of the order of a few μs.

The theory of the formation of LIG in gases and of their specific properties was presented by the author in a number of previous articles [5–7, 11, 13]. Papers [7, 11, 13] are devoted to pure electrostrictive gratings, which are formed at any wavelength of the light source. Fundamentals of the formation of electrostrictive gratings are given by Boyd [1].

Electrostrictive gratings are mainly built up from sound waves. They are generated in the overlap volume of the beams of the light source and propagate in the two opposite directions normal to the fringes of the electric field. In [13], the effects of the mutual coherence of the grating forming beams on the grating amplitude and of the processes of the

W. Hubschmid (✉)
Paul Scherrer Institut, 5232 Villigen PSI, Switzerland
e-mail: walter.hubschmid@psi.ch
Fax: +41-56-3102199

dissipation of the grating (viscosities, thermal conductivity) were calculated, and they were compared and validated with experimental results. The application of electrostrictive LIG for the measurement of sound velocities was described in [7]. Paper [11] was devoted to the formation of electrostrictive LIG in gas flows. Here, general relations for the signal intensity of a probe beam that is diffracted from an LIG are given. In particular, effects of a reference beam in a heterodyne arrangement, of a finite transit time of the acoustic waves, and of a probe beam, which encounters the grating not in its centre, are included.

Heat release effects in pure electrostrictive gratings and in absorbing media (with respect to the source beams) were discussed in [6]. The heat release from the absorption of light results from collisional relaxation of the state excited by the light source. With "thermal" LIG, in contrast to LIF (laser-induced fluorescence), the effect of the so-called quenching process is detected. Since usually more energy is released in this process than by fluorescence, LIG represents a rather sensitive measurement technique for detection of rare species, cp. the recent investigation of Kozlov and Radi [8]. Thermal LIG, in contrast to pure electrostrictive LIG, are not only formed by counter-propagating sound waves. In addition, also a stationary density wave with equal amplitude is built up, the so-called Rayleigh mode. (This mode is produced in pure electrostrictive gratings only by the processes of dissipation.) In [6], an overview on the phenomenology of combined electrostrictive and thermal gratings is given. In the derivations, it was still assumed that heat release is a fast process, compared with thy typical time scales observed in the given type of LIG. This time scale is usually given by the propagation time of the sound wave from one grating fringe to another and is thus responsible for the period of the oscillation of the LIG signal. The duration of this period is, in the setup with narrow angles between the beams, of the order of 50 to 100 ns.

In [4], it was demonstrated that the time-resolved LIG technique can be applied to slow heat release processes. The case study was the formation of LIG in pure $O_2$ and in $O_2$ mixed with $CO_2$. $O_2$ molecules were excited by means of beams of an OPO to the long-living electronic singlet $b^1\Sigma_g^+(v'=0)$ state, following the spatially periodic pattern of the electric field intensity. Paper [4] also contains results on the absorption spectrum of $O_2$ in the investigated range. The scope of these investigations was extended in [5]. Grating formation and the temporal evolution of the LIG for heat release processes of an arbitrary time scale are calculated here, including thus effects of slow relaxation processes. The effect of subsequent relaxations, which are assumed to be the case in the $O_2$–$CO_2$ system, is taken into account in this paper, and also relations how the populations of the various states evolve in time are given. As the electric polarizabilities in the various states under consideration differ, population changes of states also contribute to the grating amplitude. They represent the so-called population gratings.

The present paper continues the investigations of [5] on the temporal evolution of LIG in pure $O_2$ and in mixtures of $O_2$ with $CO_2$ after excitation of the $O_2$ molecules to the singlet state $b^1\Sigma_g^+(v'=0)$. Modeling the formation of the population grating is extended. The main achievement is the numerical simulation for such processes and its validation with experimental data. Contributions to the LIG, which are included in the model, originate from heat release and electrostriction, giving rise to a density change in the medium, and from the variation of the polarizabilities of the excited molecular states. For the analysis of the experimental data, a three-step relaxation process of the excited $O_2$ molecules is assumed: First, thermal equilibrium with respect to the rotational states is formed. This process happens within nanoseconds. The second step is the electronic relaxation to the $^1\Delta_g$ state. This process is rather slow in pure oxygen; however, it is strongly enhanced by $CO_2$, which in our experiments was added to the $O_2$ in various concentrations (cp. Sect. 4). After the collision, the $O_2$ and the $CO_2$ molecules are vibrationally excited. Only a small amount of the total absorbed radiation energy is released in this step, cp. the presentation of Wayne [14]. Various parallel relaxation processes in this step, in order to still be able to handle the model in simulations, are summarized by a single value for the relaxation rate. From compilation of results of various authors, this rate, with a rather large uncertainty, is noted in [14]. The third step in the modeling is the final relaxation, comprising many different slow processes and releasing the bulk of the excitation energy. Again in this paper, it is assumed that this step in the relaxation can be approximated by a single rate.

The investigation presented in [3] is closely related to the work described here and in the previous papers [4, 5]. There, relaxation processes in pure $O_2$ at various pressures up to 160 bar, and after excitation of some of the $O_2$ molecules to the $b^1\Sigma_g^+(v'=0)$ state are described in great detail, experimentally and theoretically.

## 2 Modeling

The diffraction of a probe beam at a non-absorbing laser-induced grating is obtained by solving the wave equation for the electric field

$$\Delta E - \frac{n^2+\Delta\chi}{c^2}\frac{\partial^2 E}{\partial t^2} = 0 \tag{1}$$

with spatially dependent laser-induced real variation $\Delta\chi$ of the electric susceptibility [1]. It follows from (1) that the intensity of the diffracted beam, and therewith the diffraction efficiency, is proportional to the square $(\Delta\chi)^2$.

In general, the electric susceptibility $\chi$ of a dilute gas mixture can be expressed by the polarizabilities of the various molecular states present in the medium. Thus,

$$\chi = \frac{N_0}{\varepsilon_0}\left[\alpha_0\left(1-\sum_1^n f_i\right)+\sum_1^n f_i\alpha_{0,i}\right]+\frac{1}{\varepsilon_0}\sum_1^s N_j\alpha_j. \quad (2)$$

The first term of the RHS of (1) contains the contribution to $\chi$ from the species in the gas mixture which is excited by the laser. The 0-indexed quantities refer to this species: $N_0$ is the number of molecules per volume, $\alpha_0$ is the polarizability of the ground state, $\alpha_{0,i}$ are the polarizabilities of the excited states, $i = 1 \ldots n$, and $f_i$ are the mole fractions of the excited states. The second term of the RHS of (1) contains the contribution to $n$ from the other species in the gas mixture, with the corresponding quantities $N_j$ and $\alpha_j$. For simplicity, we do not consider in (2) that excited states also of these other species are formed in the course of the relaxation process. Note, however, the remark at the end of this section.

We calculate variations of $\chi$ by deriving (2) with respect to the independent variables $f_i$ and the density $\rho$. This is noted here for our case of only two species present in the mixture:

$$\Delta\chi = \frac{N_0}{\varepsilon_0\rho}\left(\alpha_0+\frac{p_1}{p_0}\alpha_1+\sum_1^n f_i\,\Delta\alpha_{0,i}\right)\Delta\rho + \frac{N_0}{\varepsilon_0}\sum_1^n \Delta\alpha_{0,i}\,\Delta f_i, \quad (3)$$

where $\Delta\alpha_{0,i} \equiv \alpha_{0,i} - \alpha_0$. In our case, the sum-term in the coefficient to $\Delta\rho$ is negligible because of small saturation. Thus the coefficient of the $\Delta\rho$-term is known from tables in literature. For the polarizability of oxygen (in the ground state), one finds $\alpha_0 = 1.8 \times 10^{-40}\ (\mathrm{A\,s})^2\,\mathrm{kg}^{-1}\,\mathrm{s}^2$. The polarizability of $CO_2$ is $\alpha_1 = 2.93 \times 10^{-40}\ (\mathrm{A\,s})^2\,\mathrm{kg}^{-1}\,\mathrm{s}^2$.

The second term of (3) is the contribution from the change in populations of excited states. We denote it by $\Delta\chi_{\mathrm{pop}}$. With $N_{0,i} \equiv \Delta f_i N_0$, one has

$$\Delta\chi_{\mathrm{pop}} = \frac{1}{\varepsilon_0}\sum_1^n \Delta\alpha_{0,i}N_{0,i}. \quad (4)$$

In order to obtain the diffraction efficiency of the induced grating, the variations of the density and of the concentrations of excited molecules in the medium have therefore to be known.

For modeling $\Delta\chi_{\mathrm{pop}}$, the temporal evolution of the populations of the state excited by the light source and of the states reached in the first relaxation step is considered. The values of the polarizabilities of these states are determined in our approach by experiment. One obtains

$$N_{0,1}(t,x) = \cos(qx)N_{0,1}(t=t_0) \times \exp\big[-(\lambda_1+\vartheta)(t-t_0)\big]\Theta(t-t_0), \quad (5)$$

$$N_{0,2}(t,x) = \cos(qx)N_{0,1}(t=t_0)\frac{\lambda_1}{\lambda_1-\lambda_2} \times \big\{\exp\big[-\lambda_2(t-t_0)\big]-\exp\big[-\lambda_1(t-t_0)\big]\big\} \times \big[\exp\big[-\vartheta(t-t_0)\big]\big]\Theta(t-t_0). \quad (5')$$

In (5, 5′), $N_{0,1}(t,x)$ and $N_{0,2}(t,x)$ are the (temporal evolutions of the) enhancements of the numbers of molecules per volume for the $b^1\Sigma_g^+$ state and the $^1\Delta_g$ state, respectively, at the grating fringes, compared with the mean numbers of molecules per volume over a spatial period of the grating. Furthermore, $q$ is the grating vector, $\lambda_1$ is the rate of the heat release in the electronic de-activation, and $\vartheta$ is the mass diffusion constant. By mass diffusion the spatially sinusoidal variations of the populations of the ground state and of the excited states decrease exponentially in time. The final relaxation processes are approximately taken into account by an average relaxation rate $\lambda_2$. The quantity $\lambda_2$ is assumed to depend on the concentration of both $CO_2$ and $O_2$. This is a consequence of the fact that various types of collisions contribute to the third and final step of the heat release. Actually, with increasing concentration of $CO_2$, the probability of collisions between two $CO_2$ molecules rises quadratically.

The variation of the density $\Delta\rho$ in (3) contains three contributions, which refer to the three steps of heat release of the excitation energy of the $O_2$ molecules. We distinguish them by inserting indices, i.e., the various contributions are denoted by $\Delta\rho_1$, $\Delta\rho_2$, and $\Delta\rho_3$. In the first term, $\Delta\rho_1$, the effect of electrostriction on the formation of the LIG is added. The calculation is done by solving with appropriate source terms the equations which are obtained for disturbances around equilibrium from the fluid dynamic equations [1]. This procedure is described in detail in [5]. We note here the result in zeroth order of $\beta_1/\varpi$, $\beta_2/\varpi$:

$$\Delta\rho_1(t,x) = -\frac{\zeta h\nu\beta_p N_{0,1}(t=t_0)}{c_p}\cos(qx)\Theta(t-t_0) \times \exp\big[-\beta_2(t-t_0)\big] - \exp\big[-\beta_1(t-t_0)-(t-t_0)^2/\tau^2\big] \times \big[\cos\big[\varpi(t-t_0)\big] + (\gamma_e/\zeta\gamma_a)\sin\big[\varpi(t-t_0)\big]\big]. \quad (6)$$

The second term in the curly brace gives the contribution to the grating from the counter propagating sound waves. The effect of the propagation of the sound waves out of the probe volume is described by a Gaussian, which contains what we

call the transit time $\tau$. This parameter indicates the duration after which, in average, the sound waves have left the observation volume. It is determined by experiment. The further symbols used in (6) are the following: $\gamma_e$ for the electrostrictive coupling constant (it coincides with the electric susceptibility); $\gamma_a$ for the absorptive coupling constant defined to be $\gamma_a = 2ancv\beta_p/c_p q$; $\zeta$ for the fraction of the total heat release, which is liberated in the first relaxation step; $\alpha$ for the optical absorption coefficient at the excited line of $O_2$; $\nu$ for the frequency of the light source of excitation; $\beta_1$ for the dissipation constant of the sound waves. This constant contains the effect from thermal diffusion and from viscosity, including the bulk viscosity. Furthermore, $\beta_2$ is the dissipation constant for the isobaric density wave (Rayleigh mode), which is given by the thermal diffusivity alone; $t_0$ is the instant of peak field strength in the measurement volume; $\varpi$ is the acoustic (angular) frequency; $v = (\partial p/\partial\rho)_S^{1/2}$ is the adiabatic sound velocity; $c_p$ is the specific heat capacity at constant pressure; and $\beta_p = -(1/\rho)(\partial\rho/\partial T)_p$ is the thermal expansion coefficient at constant pressure.

In (6), the quantity $N_{0,1}(t = t_0)$ introduced in the expressions for the populations, (5, 5′), appears again. Actually, the enhancement of the electric field intensity $I_{\text{var}}$ along the grating, compared to its average value over a spatial period of the grating, enters the equations that describe the formation of the grating, cp. [5]. $I_{\text{var}}$ is given there in the form $I_{\text{var}} = 2A\cos(qx)\delta(t - t_0)$, defining thereby the parameter $A$. (The electric field intensity by definition is the square of the field strength averaged over one period: $I = 1/T\int_0^T E^2\,dt$.)

The enhancement $N_{0,1}(t = t_0)$ of the number of excited molecules per volume in the grating fringes can be calculated from the variation of the field intensity $I_{\text{var}}$ using the optical absorption coefficient $\alpha$. Actually, at $x = 0$,

$$N_{0,1}(t = t_0) = \int \dot{N}\,dt = \frac{\alpha c\varepsilon_0}{h\nu}\int I_{\text{var}}(x = 0)\,dt = \frac{2A\alpha c\varepsilon_0}{h\nu}. \tag{7}$$

Here the expression $u = \varepsilon_0 I$ for the energy density of the electromagnetic field was inserted.

The temporal evolution of the density variation $\Delta\rho_2$ in the second and slow process of relaxation was also already given in [5]. Expressing the field intensity again by the quantity $N_{0,1}(t = t_0)$, $\Delta\rho_2$, up to first order of $\beta_1/\varpi$, $\beta_2/\varpi$, and $\lambda_1/\varpi$, is given by

$$\Delta\rho_2(t, x) = -\frac{\lambda_1\zeta_1 h\nu\beta_p N_{0,1}(t = t_0)}{c_p}\cos(qx)\Theta(t - t_0) \times \frac{\exp[-(\lambda_1 + \vartheta)(t - t_0)] - \exp[-\beta_2(t - t_0)]}{\beta_2 - (\lambda_1 + \vartheta)}. \tag{8}$$

where $\zeta_1$ is the fraction of the total heat release, which is liberated in the second relaxation step.

The density variation $\Delta\rho_3$ for Step 3 in the chain of heat releases is again taken from [5]. (Correction: In this article, the factor $\lambda_1/(\lambda_1 - \lambda_2)$ is missing on the right-hand side of the intermediate (19).) In the modeled amplitude, we include only terms of lowest order in $\beta_1/\varpi$, $\beta_2/\varpi$, and $\lambda_1/\varpi$. Thus,

$$\Delta\rho_3(t, x) = \frac{\lambda_1\lambda_2\zeta_2 h\nu\beta_p N_{0,1}(t = t_0)}{(\lambda_1 - \lambda_2)c_p}\cos(qx)\Theta(t - t_0) \times \left\{\frac{\exp[-(\lambda_1 + \vartheta)(t - t_0)] - \exp[-\beta_2(t - t_0)]}{\beta_2 - (\lambda_1 + \vartheta)} - \frac{\exp[-(\lambda_2 + \vartheta)(t - t_0)] - \exp[-\beta_2(t - t_0)]}{\beta_2 - (\lambda_2 + \vartheta)}\right\}. \tag{9}$$

With the relations (4) to (9), the quantities occurring in (3) are given in explicit form. The signal intensity obtained from modeling is in the next step fitted by determining the least-square deviation to the experimentally observed temporal evolution of the LIG signal. In this way, possibly, optimized values for parameters $\zeta$, $\zeta_1$, $\lambda_2$, $\Delta\alpha_{0,1}/\alpha_0$, and $\Delta\alpha_{0,2}/\alpha_0$ can be obtained. $\Delta\alpha_{0,1}$ and $\Delta\alpha_{0,2}$ are the variations of the polarizability of $b^1\Sigma_g^+$ and $^1\Delta_g$ (here including the state of the collision partner molecule $CO_2$), respectively, compared with the electronic and vibronic ground state. By the fitting procedure, in addition, among other parameters, the overall factor for the scattering amplitude and the transit time $\tau$ of the sound waves are determined. The procedure of optimization and determination of physical parameters is described in more detail in Sect. 4.

## 3 Data acquisition

The experimental data on the temporal evolution of LIG, in various mixtures of $O_2$ and $CO_2$ (at room temperature) as medium, were obtained previously with the set-up described in [5]. The different concentrations of both, $O_2$ and $CO_2$, investigated in the experiments are noted in Sect. 4. A scheme of the set-up is shown in Fig. 1. The two beams used to induce the transient grating in the medium (various mixtures of $O_2$ and $CO_2$) were provided by a single-longitudinal-mode optical parametric oscillator (OPO, Continuum HRL-100Z). The OPO was operated at the wavelength 760.4 nm of the $^{\text{R}}$R(11) line of the $b^1\Sigma_g^+(v' = 0)$ state excitation of $O_2$. The pulse length was about 5 ns with a bandwidth smaller than 500 MHz. Focused by a lens ($f = 1000$ mm), the two excitation beams overlapped each other at the focus located in a sample cell. The angle $\theta$ formed by the excitation beams was about 1.1°. The accurate value of the grating

constant $q$ was derived from the measured period $T$ of the LIG signal. It varied in very small amounts, because of new adjustments, during the various measurements.

A beam of a cw $Ar^+$ laser (Innova 70-4) read out the laser-induced grating. A second lens ($f = 1000$ mm) was used to focus the counterpropagating beam of the $Ar^+$ laser in a planar backward phase matching geometry. The power of the $Ar^+$ laser was 1.7 W running in single line mode at $\lambda = 514.5$ nm. To allow for time resolved acquisition of single pulse LIG signals, a digitizer (Tektronix TDS 544A) with a bandwidth of 500 MHz and a sampling rate of $2 \times 10^9$ $s^{-1}$ was used. Experimental results (Figs. 2 to 6) are shown in the next section.

Saturation is small for the given experimental parameters. Using estimated values for the irradiated energy per area and tabulated values of the optical absorption coefficient (from [14]), one finds that the OPO pulse excites about a fraction of 0.004 of the $O_2$ molecules to the $b^1\Sigma_g^+(v' = 0)$ state.

## 4 Optimization procedure and determination of physical parameters

A Matlab routine was written for the optimization procedure and determination of unknown parameters. This routine was adapted to the various cases that were considered. The first case was an LIG formed in pure $O_2$ (of 0.973 bar). Figure 2a shows the temporal evolution of the diffraction efficiency of the grating up to about $t - t_0 = 4$ µs; the time slot up to $t - t_0 = 1.5$ µs is given in Fig. 2b. Least-square optimization of the modeled function for the LIG intensity to the experimental data, with specifying parameters to be determined, is simplified here since $\lambda_1$ is very small in the case of pure $O_2$ [14] and can therefore be set to zero. Thus, in this case, the energy fraction $\zeta$ and the variation of

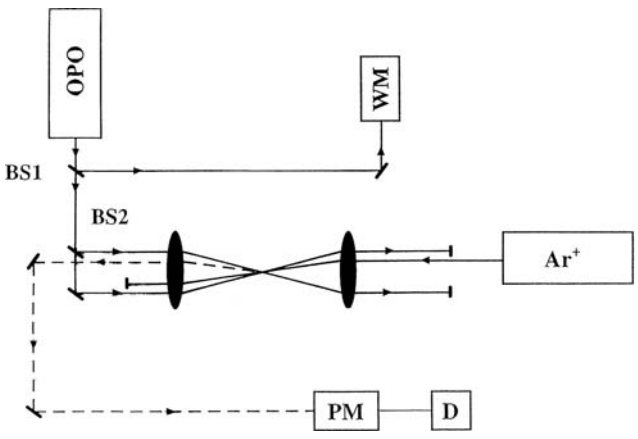


**Fig. 1** Experimental set-up. $Ar^+$: Argon laser; BS1: Beamsplitter with R = 10%; BS2: Beamsplitter with R = 50%; WM: wavemeter; PM: photomultiplier tube; D: digitizer

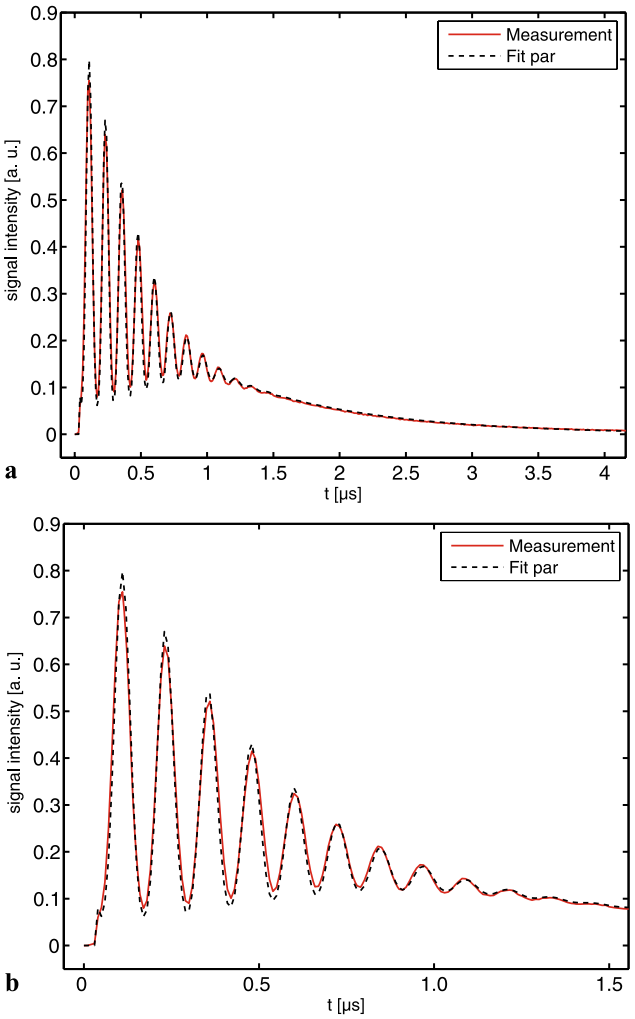


**Fig. 2** Temporal evolution of a single-pulse LIG signal for the $^R$R(11) transition obtained in pure $O_2$ of 0.973 bar, in comparison with numerical simulation. Time-slots: **a** 4 µs, **b** 1.5 µs

polarizability $\Delta\alpha_{0,1}/\alpha_0$ are the only quantities from the list of quantities mentioned at the end of Sect. 2 which have to be determined. In the procedure for the optimization chosen here, the overall factor for the signal intensity and the quantity $\zeta$ were determined simultaneously. The size of the relative variation of the polarizability $\Delta\alpha_{0,1}/\alpha_0$ was guessed from the height of the jump of the signal intensity at $t = t_0$, at the time where the OPO pulse reaches the grating. We obtain $\Delta\alpha_{0,1}/\alpha_0 = -0.045$ as an optimal value, with an error of about ±10%. (Values of –0.041 and –0.049 for $\Delta\alpha_{0,1}/\alpha_0$ gave worse agreement.) For the energy fraction released by the relaxation of rotational states, we obtain $\zeta = 0.00163$. This corresponds to $\gamma_e/\zeta\gamma_a = 0.99$, which is close to the value calculated in [6], $(\gamma_e/\zeta\gamma_a)_{\text{calc}} = 1.02$; the parameter $\gamma_e/\zeta\gamma_a$ indicates the relative strength of electrostrictive and thermal contribution to the formation of the LIG caused by the density variation $\Delta\rho_1$, cp. (6). By varying the optimized value, the error in determining $\zeta$ is estimated to be about 5%.

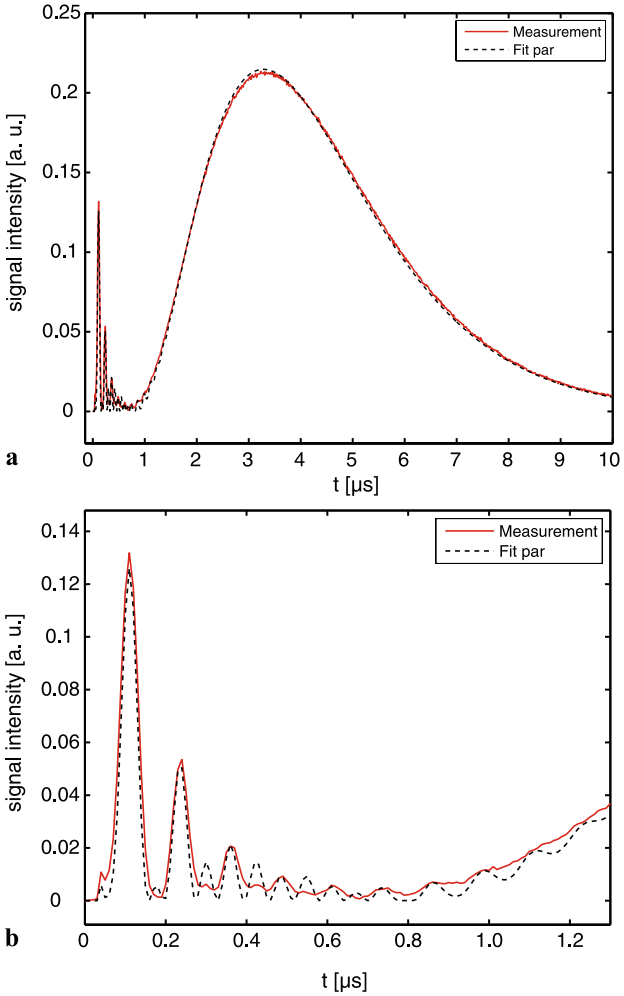


**Fig. 3** Temporal evolution of a single-pulse LIG signal for the $^{R}$R(11) transition obtained in a mixture with 0.735 bar $O_2$ and 0.197 bar $CO_2$; in comparison with numerical simulation from three-step relaxation model. Time slots: **a** 10 μs, **b** 1.2 μs

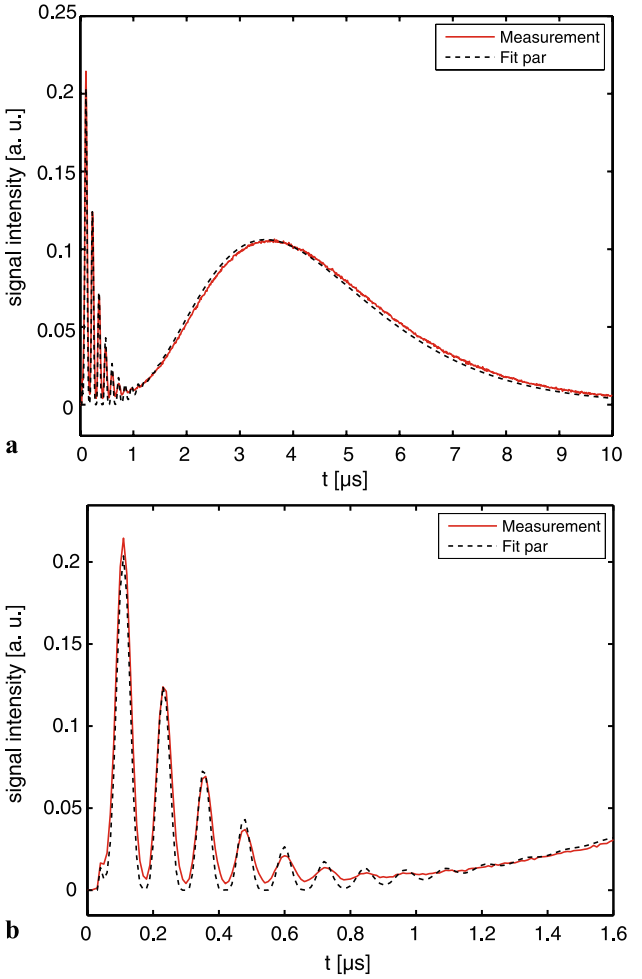


**Fig. 4** As Fig. 3; with 0.844 bar $O_2$ and 0.101 bar $CO_2$, and time slots in **a** 10 μs, **b** 1.2 μs

The parameters $\zeta$ and $\Delta\alpha_{0,1}$ determined in this way are then used for the further cases, where $O_2$ is mixed with $CO_2$.

Within the same procedure, the acoustic frequency $\nu$, the transit time $\tau$, and the time $t_0$ were also determined. The frequency $\nu$ was obtained to be $\nu = 7.97$ MHz. This corresponds to a period $T = 125.5$ ns, a fringe spacing $\Lambda = 40.3$ μm, and a grating vector $q = 1.56 \times 10^5$ m$^{-1}$. The transit time was determined to be $\tau = 0.69$ μs with an uncertainty of about 10%; this corresponds to a diameter in the focus of about 0.2 mm. The transit time was correspondingly adapted to the experiments in mixtures of $O_2$ with $CO_2$. Physical properties, including the sound velocity, were taken from tables [10]. (In principle, LIG allows a determination of the sound velocity. However, as the measurement of the crossing angle $\theta$ between the beams has limited accuracy, a reference value of the sound velocity is used, $v = 327$ ms$^{-1}$, and the quantities $\Lambda$ and $q$ are obtained in this way from the acoustic frequency.) For the bulk viscosity $\eta_b$ which enters the parameter $\beta_1$, we used the values (not yet published) from separate experiments with pure electrostrictive LIG. For $O_2$ at the given acoustic frequency, we found that $\eta_b = 0.73\eta_s$ ($\eta_s$, shear viscosity). The values for the dissipation constants $\beta_1$ and $\beta_2$ are $\beta_1 = 4.97 \times 10^5$ s$^{-1}$ and $\beta_2 = 5.23 \times 10^5$ s$^{-1}$. The electrostrictive coupling constant is $\gamma_e = 0.000479$. The optical absorption coefficient at the $^{R}$R(11) line was taken from [12]. In the given case, it is $\alpha = 0.0579$ m$^{-1}$.

In the second step, experimental data for the temporal evolution of the LIG signal in mixtures of 0.844, 0.74, 0.608, and 0.439 bar $O_2$ with 0.101, 0.197, 0.312, and 0.490 bar $CO_2$, respectively, were compared with the data obtained from numerical simulation, using the model of Sect. 2. General features of the experimental data, which should be reproduced by the simulation, are the following: (a) The grating decays faster with increasing concentration of $CO_2$ in the initial phase (up to about $t - t_0 = 0.8 \ldots 0.4$ μs, depending on the $CO_2$ content); (b) in mixtures with $CO_2$, the grating reflectivity rises again after the first decay, after about

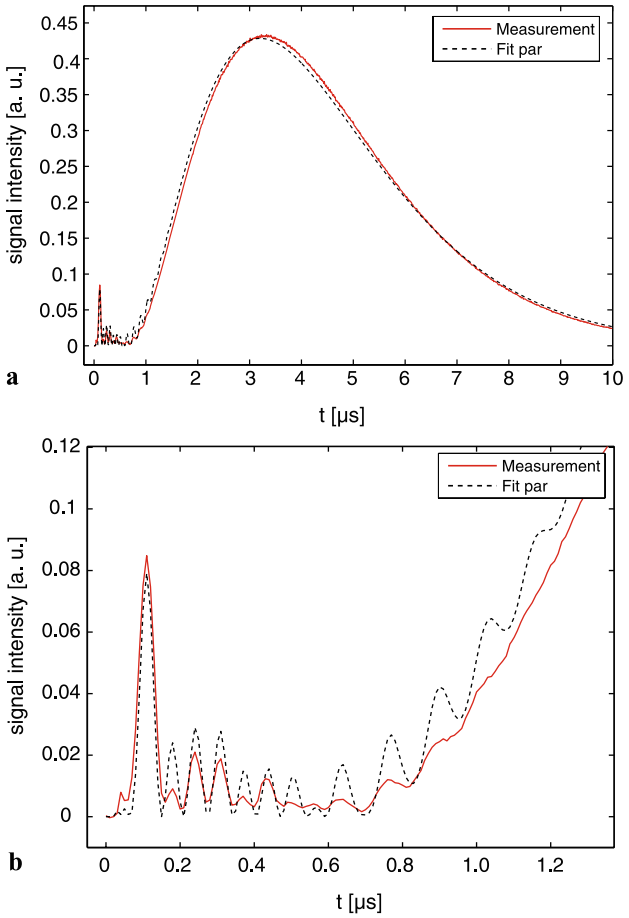


**Fig. 5** As Fig. 3; with 0.608 bar $O_2$ and 0.312 bar $CO_2$, and time slots in **a** 10 μs, **b** 1.2 μs

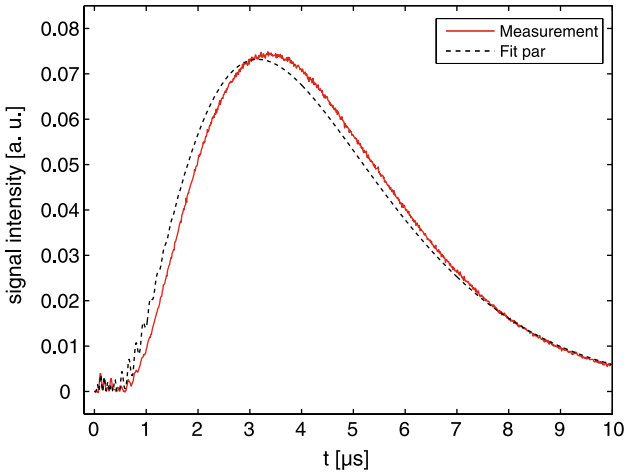


**Fig. 6** As Fig. 3; with 0.439 bar $O_2$ and 0.490 bar $CO_2$, time slot 10 μs

$t - t_0 = 1.0 \ldots 0.7$ μs, before it finally decays because of mass diffusion, at about the time $t - t_0 = 4$ μs.

The following procedure for the optimization and determination of physical quantities was chosen. First, the case of 0.74 bar $O_2$ and 0.20 bar $CO_2$ was considered. Here, various values of $\Delta\alpha_{0,2}/\alpha_0$ were assumed; the optimization was done with respect to the parameters $\zeta_1$ and $\lambda_2$. Fine tuning led to values for the overall constant of the LIG signal intensity and to values for the mass diffusion constant $\vartheta$. It was found that the values of $\vartheta$ obtained from solving the diffusion equation for infinite planes and taking values for the diffusion coefficients from [9] (for self diffusion of $O_2$ and for $O_2$–$CO_2$ diffusion) were larger by about 20% than the values obtained directly from our experiment. Values for the other dissipation constants ($\beta_1$ and $\beta_2$) were taken from [10]; the bulk viscosity was again determined by a separate experiment with pure electrostrictive LIG. In general, arithmetic means with respect to pressures were used for the physical constants in the mixtures of $O_2$ and $CO_2$.

The relaxation constant $\lambda_1$ for the quenching of the state $b^1\Sigma_g^+(v' = 0)$ was taken from [14]. $\lambda_1$ of pure $O_2$ is very small; therefore the rate $\lambda_1$ is in very good approximation proportional to the concentration of $CO_2$. The tables of [14] give the value $\lambda_1$ (0.1 bar $CO_2$) $= 10^6$ s$^{-1}$ with an error of approximately ±30%. Variations around the given mean value led in tendency to worse agreement between experiment and model. For the second variation of polarizability, the value $\Delta\alpha_{0,2}/\alpha_0 = 0$ gave best agreement between experiment and model. From this $\zeta_1 = -0.0064$ is obtained. Values for $\Delta\alpha_{0,2}/\alpha_0$ in about the interval $[-0.1, 0.1]$ are, however, not excluded.

The values of $\zeta_1$ and $\Delta\alpha_{0,2}/\alpha_0$ determined with this first experiment were then used for the simulation of the experimental data for other pressures of $O_2$ and $CO_2$. Thus, only the relaxation parameter $\lambda_2$ had still to be determined in these optimizations. The overall factor for the LIG signal intensity and the mass diffusion constant were determined separately, by trial and error. As a general result, we obtain a monotonic variation for the (average) rate $\lambda_2$, which strongly increases with increasing pressure of $CO_2$. The values are with errors of the orders of about ±10%: $\lambda_2 = 0.94 \times 10^4$ s$^{-1}$ (for the case with 0.101 bar $CO_2$), $\lambda_2 = 1.00 \times 10^4$ s$^{-1}$ (for 0.197 bar $CO_2$), $\lambda_2 = 1.38 \times 10^4$ s$^{-1}$ (for 0.312 bar $CO_2$), and $\lambda_2 = 2.39 \times 10^4$ s$^{-1}$ (for 0.490 bar $CO_2$).

Results of the simulations in comparison with the experimental data, for the various cases considered, are shown in Figs. 3 to 6. Again, different time windows of the processes are depicted. The most striking features of the experimental data are well reproduced by the model; i.e., the decrease of the oscillations during the first part of the signal, which is strongly dependent on the $CO_2$ pressure, and the rise of the signal in the final part in the experiments with $CO_2$ added to the $O_2$. On the other hand, the simulation overemphasises oscillations of the signal intensity for about the time $t - t_0 > 0.8$ ms, which are only faintly visible in the data; cp. especially the results for 0.31 bar and 0.49 bar $CO_2$. This

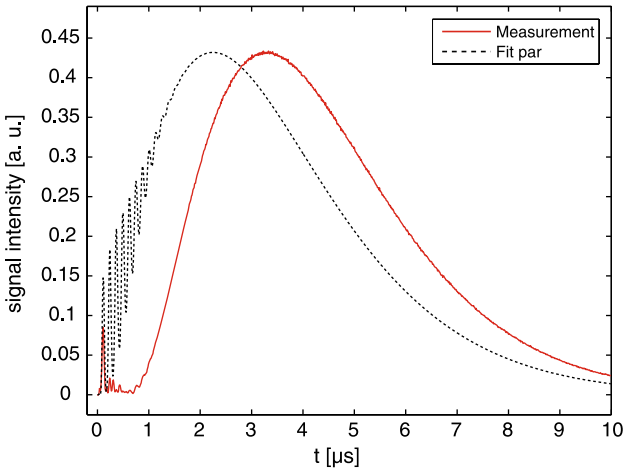


**Fig. 7** Simulation of the LIG signal for a fictitious case with only two steps of heat release, for a mixture with 0.608 bar $O_2$ and 0.312 bar $CO_2$, together with the experimental data

discrepancy disappears, however, by reducing by about 30% the transit time, which was determined, see above, by the measurement in pure $O_2$ and correspondingly adapted to the cases containing $CO_2$.

Furthermore, in the case of highest $CO_2$ content, the final rise of the LIG intensity happens earlier in the simulation than in experiment, by about 0.2 μs. In the detailed behavior of the LIG intensity, there are some additional discrepancies, which can possibly be explained by, first, that only one relaxation rate per step was assumed and, second, by missing the best optimization values in the iterative procedure. To do a simultaneous optimization for all parameters requested turned out not to be feasible.

Figure 7 shows for the case with 0.608 bar $O_2$ and 0.312 bar $CO_2$, together with the experimental data, the result of a simulation considering a chain of only two relaxation processes. In this modeling case, the second relaxation has the rate, which was, in the optimization for the full model with three processes, determined for the third relaxation. Furthermore, the second relaxation liberates all the excitation energy that is not released in the first relaxation process. A very strong difference between data and "model" arises already after about 0.4 μs. Although the inverse relaxation rate of the second process in the real model is of the order of 0.3 μs, it delays the heat release of the third relaxation process by about 1 μs. This illustrates that the intermediate medium fast process, although releasing only very little energy, changes the behavior of the temporal evolution of the LIG intensity strongly. The reason for this effect is, as already mentioned in [5], that the last relaxation process rises, in contrast to the second process, not linearly with time but only quadratically and that the amplitudes of these two processes have different signs.

Actually, if one separately depicts, for the case with 0.608 bar $O_2$ and 0.312 bar $CO_2$, the calculated functions $\Delta\rho_2$ and $\Delta\rho_3$ ((8) and (9), respectively), which are the two main contributions to the LIG amplitude in the middle and later phase, one observes that: (a) $\Delta\rho_2$ rises linearly with time first, and it reaches its (rather flat) maximum at around $t - t_0 = 0.9$ μs; the final decline is (mainly) a consequence of that the respective rate of heat release diminishes exponentially with time, with the decay constant $\lambda_1 = 3.1 \times 10^6\ s^{-1}$; (b) $\Delta\rho_3$ (with negative sign) starts slowly (quadratically) at $t - t_0 = 0$; it equals $\Delta\rho_2$, up to the sign, at around 0.75 μs. The absolute value of $\Delta\rho_3$ reaches its maximum at around 2.8 μs, i.e., rather early compared to the relevant (average) decay constant $\lambda_2 = 1.38 \times 10^4\ s^{-1}$. This is due to the mass diffusion that proceeds at a rate given by the constant $\vartheta = 3.5 \times 10^5\ s^{-1}$.

## 5 Summary and conclusions

Relaxations processes in mixtures of $O_2$ with $CO_2$ after the excitation of $O_2$ molecules to the $b^1\Sigma_g^+(v' = 0)$ state were studied with the time-resolved LIG technique. To model the relaxation, three subsequent steps of heat releases were assumed. In this way, reasonably good agreement between experimental data and the simulation of the LIG signal was obtained.

In particular, the model reproduces the experimental finding that the signal in the first phase decays faster with growing concentration of $CO_2$ and that it rises again in a later phase. These effects are consequences of the relative strengths of the subsequent relaxation processes. Some discrepancies remain between simulation and experimental data. It is supposed that they can be traced back mainly to the simplification in the model, by using only one average relaxation rate for each of the subsequent processes. Discrepancies grow with increasing concentration of $CO_2$; this may be due to the quadratically enhanced contribution of collisions between two $CO_2$ molecules. Another source of inaccuracy, possibly, could originate from the optimization procedure. Actually, optimization using standard Matlab routines turned out to be rather difficult because of the number of parameters involved in the optimization and, in particular, because the second population term and second density term contribute in a similar way to the grating's strength. These two terms can hardly be distinguished therefore. Thus, it cannot be excluded that a set of parameters with slightly different values exists, which would still better fit the data.

By comparison of simulation and experimental data, the fraction of energy release in the first step (relaxation with respect to rotational states) can be determined. It agrees very well with the value calculated earlier. Also, the variation of the polarizability for the OPO-excited $b^1\Sigma_g^+(v' = 0)$ state of $O_2$ and the (average) rate for the final relaxation processes can be determined in this way. Although the time scale in

our implementation of the time-resolved LIG technique is limited to a few μs, this average relaxation rate of the order of $10^4$ $s^{-1}$ could be determined. On the other hand, because of the difficulties in optimization described above, the value for the variation of the polarizability after the second relaxation and the value for the energy release in this step could not be determined in a reliable way.

By comparison of the strength of the electrostrictive grating with the instantaneously formed thermal grating and by the quenching of electronically excited states by molecular collisions, which is observable in the temporal evolution of the LIG, some information on the chemical composition of the observed medium can be obtained. For example, in the case investigated in this article, information on the relative concentration of $O_2$ and $CO_2$ can be drawn from observing the temporal evolution of the LIG. Thus, for some specific conditions, as it had been suggested in [5], in a set-up that resembles much the well-known set-up for CARS temperature measurements, time-resolved LIG can be used for local measurements of (relative) concentrations. From the present work we estimate the relative accuracy of such measurements to be in the order of a few percent.

**Acknowledgements** Help of R. Bombach, N. Tylli, and A. Denisov in preparing this paper is greatly acknowledged. I thank M. Neracher and W. Kreutner for discussions.

## References

1. R.W. Boyd, *Nonlinear Optics* (Academic Press, New York, 1992)
2. H.J. Eichler, P. Günther, D.W. Pohl, *Laser-Induced Dynamic Gratings* (Springer, Berlin, 1986)
3. B. Hemmerling, D. Kozlov, Chem. Phys. **291**, 213 (2003)
4. B. Hemmerling, R. Bombach, W. Hubschmid, Chem. Phys. Lett. **256**, 71 (1996)
5. W. Hubschmid, B. Hemmerling, Chem. Phys **259**, 109 (2000)
6. W. Hubschmid, B. Hemmerling, A. Stampanoni-Panariello, J. Opt. Soc. Am. B **12**, 1850 (1995)
7. W. Hubschmid, B. Hemmerling, A. Stampanoni-Panariello, Appl. Phys. B **62**, 103 (1996)
8. D. Kozlov, P.P. Radi, J. Raman Spectrosc. **39**, 730 (2008)
9. Landolt-Börnstein, *Numerical Data and Functional Relationships in Science and Technology*, 6th edn., vol. II/5a (Springer, Berlin, 1969)
10. L. Medard, *Encyclopédie des Gaz* (Elsevier, Amsterdam, 1976)
11. M. Neracher, W. Hubschmid, Appl. Phys. B **79**, 783 (2004)
12. K.J. Ritter, T.D. Wilkerson, J. Mol. Spectrosc. **121**, 1 (1987)
13. A. Stampanoni-Panariello, B. Hemmerling, W. Hubschmid, Phys. Rev. A **51**, 655 (1995)
14. R. Wayne, in *Singlet $O_2$, vol. 1. Physical-Chemical Aspects*, ed. by A.A. Frimer (CRC Press, Boca Raton, 1985)
15. Y. Yan, K.A. Nelson, J. Chem. Phys. **87**, 6240 (1987)